

# Extraordinary physical properties of superconducting YBa<sub>1.4</sub>Sr<sub>0.6</sub>Cu<sub>3</sub>O<sub>6</sub>Se<sub>0.51</sub> in a multiphase ceramic material

V. Grinenko<sup>a</sup>, A. Dudka<sup>b</sup>, S. Nozaki<sup>c</sup>, J. Kilcrease<sup>d</sup>, A. Muto<sup>d</sup>, J. Clarke<sup>d</sup>,  
T. Hogan<sup>e</sup>, V. Nikoghosyan<sup>f,g</sup>, I. de Paiva<sup>g</sup>, R. Dulal<sup>g</sup>, S. Teknowijoyo<sup>g</sup>, S.  
Chahid<sup>g</sup>, A. Gulian<sup>g,\*</sup>

<sup>a</sup>*Leibniz-Institute IFW-Dresden, PF 270116, Dresden, D-01171, Germany*

<sup>b</sup>*Shubnikov Institute of Crystallography of Federal Scientific Research Centre  
“Crystallography and Photonics”, Russian Academy of  
Sciences, Moscow, 119333, Russia*

<sup>c</sup>*Nanotechnology Systems Division, Hitachi High-Tech America, Inc., 2500 NE Century  
Boulevard, Hillsboro, 97124, OR, USA*

<sup>d</sup>*Hitachi High-Tech America, Inc., , Clarksburg, 20871, MD, USA*

<sup>e</sup>*Quantum Design, San Diego, 92121, CA, USA*

<sup>f</sup>*Physics Research Institute, National Academy of Sciences, Ashtarak, 0203, Armenia*

<sup>g</sup>*Advanced Physics Laboratory, Institute for Quantum Studies, Chapman  
University, Burtonsville, 20866, MD, USA*

---

## Abstract

We report on a novel material obtained by modifying pristine YBCO superconductor in solid phase synthesis via simultaneous partial substitution of Ba by Sr and O by Se. The intended stoichiometry was originally YBa<sub>2-x</sub>Sr<sub>x</sub>Cu<sub>3</sub>O<sub>7-x</sub>Se<sub>x</sub> with various values of  $x$ , among which  $x \approx 1$  yielded the best results. Simultaneous application of EDX and EBSD confirmed that Se atoms indeed enter the crystalline lattice cell. The detailed XRD analysis further confirmed this conclusion and revealed that the obtained polycrystalline material contains 5 phases, with the major phase (>30%) being a cuprate YBa<sub>1.4</sub>Sr<sub>0.6</sub>Cu<sub>3</sub>O<sub>6</sub>Se<sub>0.51</sub>. Following XRD analysis, we applied a newly developed approach which enabled us to determine the ionic positions and occupations in the cuprate phase. The obtained superconductor demonstrates unique properties, including i) two superconducting transitions with  $T_{c1} \approx 35$  K (granular surface phase) and  $T_{c2} \approx 13$  K (bulk granular phase)

---

\*Corresponding author.

*Email address:* gulian@chapman.edu (A. Gulian)

- this granular phase arrangement naturally yields the Wohleben effect; ii) reentrant diamagnetism and resistive state; iii) strong paramagnetism with Curie-Weiss behavior ( $\theta_{CW} \approx 4$  K) and the ferromagnetic phase overruled by superconductivity; iv) Schottky anomaly visible in the heat capacity data and most likely delivered by small clusters of magnetic moments. Thorough analysis of the heat capacity data reveals a strong-coupling  $d$ -wave pairing in its bulk phase (with  $2\Delta/T_c \approx 5$ ), and, most importantly, a very unusual anomaly in this cuprate. There are reasons to associate this anomaly with the quantum criticality observed in traditional cuprate superconductors at much higher fields (achievable only in certain laboratories). In our case, the fields leading to quantum criticality are much weaker ( $\sim 7-9$  T) thus opening avenues for exploration of the interplay between superconductivity and pair density waves by the wider research community.

*Keywords:* doubly-substituted YBCO, heat capacity, XRD structure analysis, Wohleben effect, reentrant diamagnetism, quantum phase transition.

---

## 1. Introduction

With the progress in science and technology the discovery of the phenomenon of superconductivity was inevitable: sooner or later helium would have been liquefied, and resistivity of metals been tested at liquid helium temperatures, which actually has been done by Kamerlingh Onnes in 1911 [1, 2]. The discovery of superconductivity in copper oxide materials was much less probable since the elemental combination  $\text{Ba}_x\text{La}_{5-x}\text{Cu}_5\text{O}_{5(3-y)}$  with  $x = 1$  and  $0.75$ ,  $y > 0$  cannot be delivered by technical progress, and is, first of all, the product of extraordinary brainwork and stubbornness of its creators [3]. This work generated more than 20,000 research articles, the most famous of them related to the Y–Ba–Cu–O superconductor with transition temperature  $T_c \approx 93$  K [4]. Qualitatively, it is a result of compositional substitute of La by Y, another representative of the same rare earth metals group in Periodic table of elements, combined with the certain variation of resultant stoichiometry. The YBCO was a phenomenal success and it became the most famous superconductor, since it swiftly crossed the liquid nitrogen barrier at ambient pressure, simplifying greatly the research in novel superconducting materials and delivering a great puzzle for theoreticians to decipher its mechanism. This finding stimulated many other cationic substitutions, which eventually

delivered higher transition temperature superconductivity in compositions Tl-Ca/Ba-Cu-O [5], Hg-Ba-Ca-Cu-O [6], and Bi-Sr-Ca-Cu-O [7] while eliminating the rare earth element in them.

Anionic substitutions in copper oxides are much less explored experimentally, though theoreticians have predicted interesting features (see, e.g., [8, 9]). Meanwhile, oxygen plays a crucial role in the copper oxide superconductivity. Recognizing importance of oxygen, there have been numerous attempts [10, 11, 12, 13, 14, 15, 16, 17, 18] to partially replace oxygen by other representatives (namely, S and Se) of the chalcogen group to which O belongs with contradicting statements. While successful chalcogen substitution is claimed in Refs. [10, 11, 12, 17, 18], the opposite (no entrance of S into the lattice) is reported in [13]. Moreover, in another work [15] it is claimed that Se goes into Y's position. Thus, in view of this ambiguity, the first task pursued in our research is to prove that Se indeed enters the crystalline structure and occupies certain O positions in the lattice. This task is complicated by the fact that the polycrystalline material under investigation is heterophase: as the analysis revealed, 5 phases are present. Nevertheless, by combining simultaneous EDX-EBSD analysis with newly suggested method of XRD analysis we were lucky to resolve this task with accuracy leaving no doubts on the validity the structural model. The crystalline lattice parameters, as well as the positions of Se in the crystalline lattice of superconducting phase, are identified. Details of our approach are given in Methods. Comparing our results with the previous reports, one can conclude that the main reason for success with chalcogen substitution is in simultaneous partial substitution of Ba by Sr - this kind of double substitution was not exercised in the past. The second part of our report addresses the unique physical properties of superconducting phase of  $\text{YBa}_{1.4}\text{Sr}_{0.6}\text{Cu}_3\text{O}_6\text{Se}_{0.51}$  based on standard set of measurements in these multiphase samples. Temperature dependence of resistance, magnetism and heat capacity reveal two superconducting transitions with  $T_{c1} \approx 35$  K and  $T_{c2} \approx 13$  K. Above  $T_{c1}$ , anomalous paramagnetism is detected with the Curie-Weiss behavior and positive Curie temperature  $\theta_{Curie} \approx 4$  K. While no ferromagnetism is visible in DC and AC magnetization, presence of magnetic moments (caused by changing the Cu-ion ligands from O to Se) can be deduced from these Curie-Weiss data. The samples demonstrate reentrant diamagnetism (the Wohleben effect) whose mechanism can be explained in combination with other measured quantities. The heat capacity studies allowed us to conclude that the lower  $T_c$ -phase, which constitutes the majority (volume phase), is of the d-wave nature. Very

interestingly, the electronic heat capacity demonstrates features which may be associated with the quantum criticality border crossing induced by magnetic field. Observed fluctuations in the AC magnetic susceptibility further confirm this conjecture. Magnetic field-induced quantum phase transitions, as well as quantum criticality in general [18], are a subject of intense research since they are related with the mechanism of high-temperature superconductivity. Thermodynamic evidence of possible field-induced border-crossing of quantum criticality in oxy-chalcogen  $\text{YBa}_{2-x}\text{Sr}_x\text{Cu}_3\text{O}_{7-x}\text{Se}_x$  superconductor constitutes the third main part of our research. Importantly, it occurs at much lower than usual magnetic fields [19, 20], and thus opens feasibility avenues for the research community.

## 2. Results

### 2.1. Composition of samples

Our results are obtained on polycrystalline ceramic samples. Initial stoichiometries with  $x = 0, 0.5, 0.75$  and  $1$  were explored. The most drastic changes compared to  $x = 0$  took place in samples with  $x = 1$ , which will be solely described in this article.

About a dozen pellets were prepared quite reproducibly (the details are presented in Methods). Their morphology is shown in Fig. 1. The difference in crystallinity of bulk and surface areas is evident from this figure. Moreover, the heterophase nature is evident in the bulk of the sample. The phase content would be one of the topics of performed exploration. However, the first task is to determine the selenium content in the material. This is a critical topic since the material was synthesized at high-temperatures (see Methods), and the ionic radius of Se being higher than O spreads doubts that it may be emanated from the material. Qualitative confirmation of Se presence was provided by TEM EDX (Fig. 2).

Quantitative EDX exploration requires flat surfaces of the material, which is not the case for the flakes in Fig. 1. For that purpose special techniques were used (see Methods) which yielded the results shown in Table 1.

The most accurate, last row in Table 1, is encouraging; however, it does not yet guarantee that Se is hosted in any of the unit cells of crystalline phases. Two more steps were taken for addressing this topic. The first of them consisted of simultaneous EBSD and EDX analysis, and the second - in the XRD exploration.

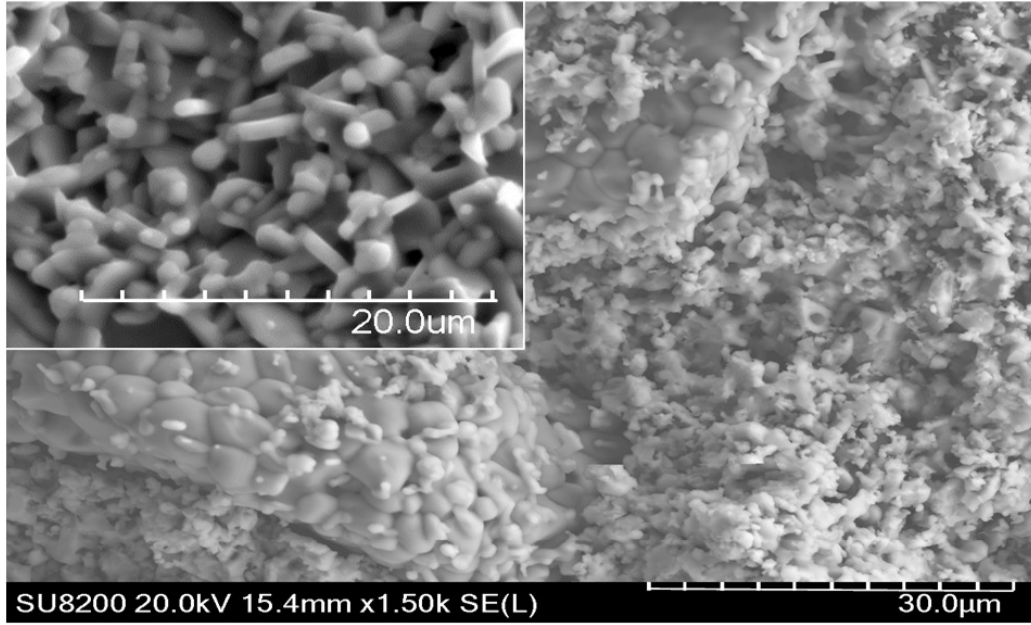


Figure 1: Morphology of freshly cleaved  $\text{YBa}_{2-x}\text{Sr}_x\text{Cu}_3\text{O}_{7-x}\text{Se}_x$  sample (by Hitachi SU8230 SEM). Inset - surface pattern (by Hitachi SU3500 SEM) of as-prepared ceramic sample.

Table 1: EDX data

Elements %(at)	O	Cu	Se	Sr	Y	Ba
Annealed surface	50.2	23.1	0.3	9.0	9.0	8.4
Cleaved surface	55.5	20.6	1.0	7.0	8.6	7.3
Ion polished surface	47.0	24.7	4.9	6.9	7.7	9.0

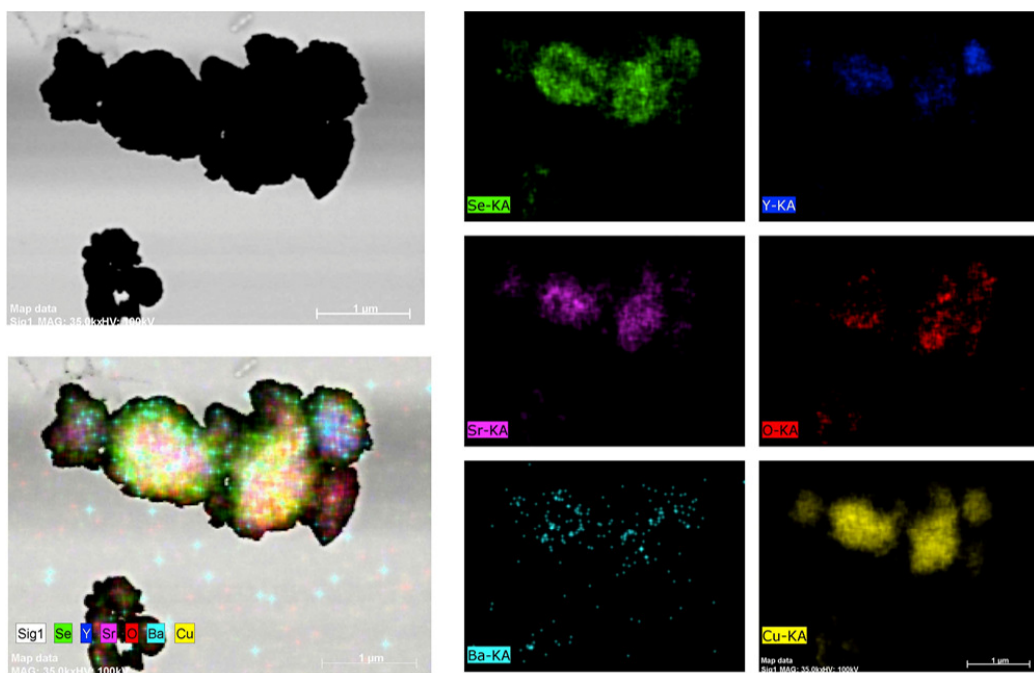


Figure 2: Abundance of Se and other constituent elements (Y, Ba, Sr, O and Cu) in thin flakes of the powdered polycrystalline  $\text{YBa}_{2-x}\text{Sr}_x\text{Cu}_3\text{O}_{7-x}\text{Se}_x$  material with the projected stoichiometry  $\text{YBaSrCu}_3\text{O}_6\text{Se}$  (transmission EDX by Hitachi HT7700 TEM with Bruker X-flash 6T|60 system).

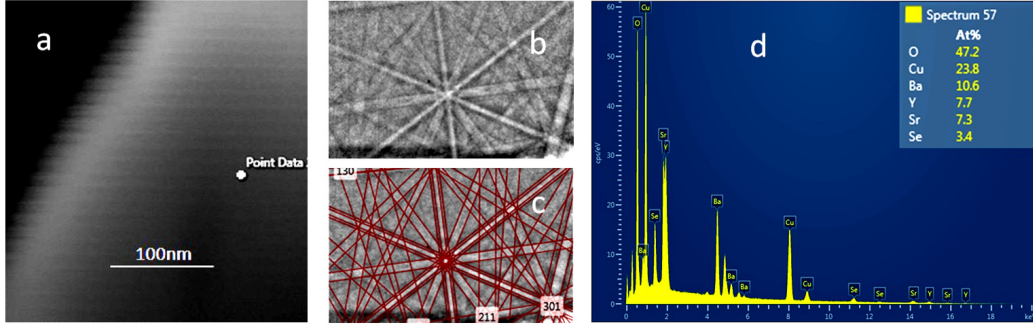


Figure 3: Compositional characterization of polycrystalline samples with the initially intended stoichiometry  $\text{YBaSrCu}_3\text{O}_6\text{Se}$  via simultaneous EBSD/EDX analysis. (a) Material's granule at  $\times 200,000$  magnification with indication of spot to which the electron beam was focused. (b) Sample orientation revealed an EBSD Kikuchi pattern. (c) EBSD database recognition of Kikuchi pattern. (d) EDX microanalysis at the same spot.

For the simultaneous EBSD and EDX analysis, the electron beam was positioned on a crystallite with magnification up to  $\times 200,000$  (Fig. 3a) so as the Kikuchi pattern is revealed (Fig. 3b) and the corresponding phase is identified (Fig. 3c). Without changing the position of the beam the corresponding EDX spectrum is acquired (Fig. 3d). Since the electron beam focusing spot is about 5 nm, and the phase identified in Fig. 3c corresponds to the  $\text{YBa}_2\text{Cu}_3\text{O}_7$  structure, one can deduce, in view of composition shown in Fig. 3d, that most likely Se enters the crystalline cells of the desired phase  $\text{YBaSrCu}_3\text{O}_6\text{Se}$ . This needs a confirmation.

X-ray diffraction indeed confirms this conclusion and provides very valuable information about the position of atomic constituents in the crystalline lattice. The results of XRD analysis are shown in Fig. 4 and Tables 2 and 3 (with more details given in Methods).

After performing Rietveld refinement, the ratio of phase contribution to X-ray scattering was identified as 30.6 : 26.0 : 24.9 : 13.7 : 4.8 *at.*% for phases 1 through 5 shown in Table 2.

Phase 1,  $\text{YBa}_{1.4}\text{Sr}_{0.6}\text{Cu}_3\text{O}_6\text{Se}_{0.51}$ , is basic for this research. Substantiation of the choice of one of three most probable models and consecutive analysis of them are described in Methods. The improvement of structural analysis criteria (such as  $R$ -factors,  $R1/wR$ , the extrema of difference Fourier synthesis,  $\Delta\rho_{\max}/\Delta\rho_{\min}$ ) takes place with each next model. Model 1: no Se in any oxygen position [21]. From this, we move to Model 2, where Se partially replaces Y [15]. Finally, we deal with Model 3, in which

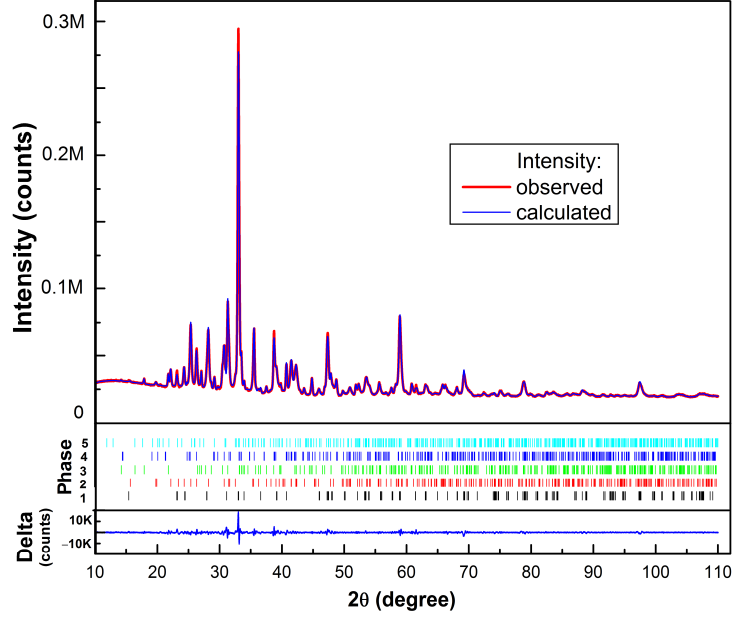


Figure 4: X-ray diffractogram of heterophase ceramic material with the initially intended stoichiometry  $\text{YBaSrCu}_3\text{O}_6\text{Se}$ . All the peculiarities of experimental profile are explained by reflections generated by 5 phases (see Table 2 and more details in Methods).

Table 2: The comparison between the literature and observed values for the proposed phases.

Phase	%	Space group, No	Chemical formula	Source	ICSD	$a$ , Å	$b$ , Å	$c$ , Å
1	30.6	$Pmmm$ , 47	$\text{YBa}_{1.4}\text{Sr}_{0.6}\text{Cu}_3\text{O}_6\text{Se}_{0.51}$	[21]	87098	3.80174(12)	3.85009(14)	11.5739(4)
				Our work	-	3.84359(4)	3.83295(6)	11.47711(18)
2	26.0	$Pnma$ , 62	$\text{BaSeO}_4$	[22]	-	8.9461(6)	5.6911(4)	7.3313(5)
				Our work	-	8.8970(2)	5.6891(2)	7.30815(18)
3	24.9	$Pna2_1$ , 33	$\text{Y}_2\text{Cu}_2\text{O}_5$	[23, 24]	067119,072058	10.8038(6)	3.49600(18)	12.4665(7)
				Our work	-	10.78668(19)	3.49389(5)	12.4404(3)
4	13.7	$Pnma$ , 62	$\text{Y}_2\text{BaCuO}_5$	[25]	063425	12.1793(7)	5.6591(5)	7.1323(4)
				Our work	-	12.30548(14)	5.67355(14)	7.03737(13)
5	4.8	$Pmn2_1$ , 31	$\text{BaCu}(\text{SeO}_3)_2$	[26]	202386	13.353(2)	5.247(1)	8.981(1)
				Our work	-	13.735(3)	5.3999(14)	8.867(2)



Table 3: Wyckoff positions, occupancies ( $q$ ), atomic coordinates ( $x/a$ ,  $y/b$ ,  $z/c$ ), and equivalent isotropic displacement parameters ( $U$ ,  $\text{\AA}^2$ ) for the basic atoms in the crystal structure of  $\text{YBa}_{1.4}\text{Sr}_{0.6}\text{Cu}_3\text{O}_6\text{Se}_{0.51}$

Atom	Wyckoff position	$q$	$x/a$	$y/b$	$z/c$	$U$
Y1	$1h$	1	0.5	0.5	0.5	0.02303(6)
Ba1 <sup>a</sup>	$2t$	0.702(1)	0.5	0.5	0.183335(4)	0.022926(8)
Sr1	$2t$	0.298(1)	0.5	0.5	0.183335(4)	0.022926(8)
Cu1	$1a$	1	0	0	0	0.03563(10)
Cu2	$2q$	1	0	0	0.348091(19)	0.03616(7)
O1	$2q$	1	0	0	0.11896(5)	0.0281(4)
O2	$2s$	1	0	0	0.40942(7)	0.0203(2)
O3	$2r$	1	0	0.5	0.35568(8)	0.0346(3)
Se4	$2k$	0.1628(5)	0.0391(8)	0	0	0.0121(3)
Se5	$1b$	0.1872(8)	0.5	0	0	0.0049(4)

<sup>a</sup> Separate refinement of parameters Ba1 and Sr1 in the full-matrix mode is possible and stable (the Sr1 atom shifts down along the coordinate  $z$  at a certain increase of its parameter  $U$ ). In the current case, we preferred avoiding insertion of additional refinement parameters in favor of keeping the larger ratio of the measurements to the number of parameters.

Se partially replaces O. For these modeling steps, we found consecutively  $R1/wR = 0.98/0.90 \rightarrow 1.09/0.93 \rightarrow 0.87/0.73$  and  $\Delta\rho_{\max}/\Delta\rho_{\min} = +0.30 / -0.48 \rightarrow +0.36 / -0.54 \rightarrow +0.17 / -0.30 \text{ e/\AA}^3$ . Final model has common criteria for accuracy based on 20001-point profile expressed by  $R_p = 1.32\%$ ,  $wR_p = 1.92\%$ ,  $GOF = 3.14$ , which confirms high enough reliability of the performed structural analysis [27]. The relevant crystalline parameters are given in Table 3.

Possible contribution of other phases is mentioned in Discussion.

## 2.2. Basic superconducting properties.

Figure 5 reveals magnetic and resistive properties of the samples.

Observations shown in Fig. 5(a-f) are complemented by the heat capacity measurements, Fig. 6.

The data presented in Fig. 5 and Fig. 6 provide very fertile grounds for discussion.

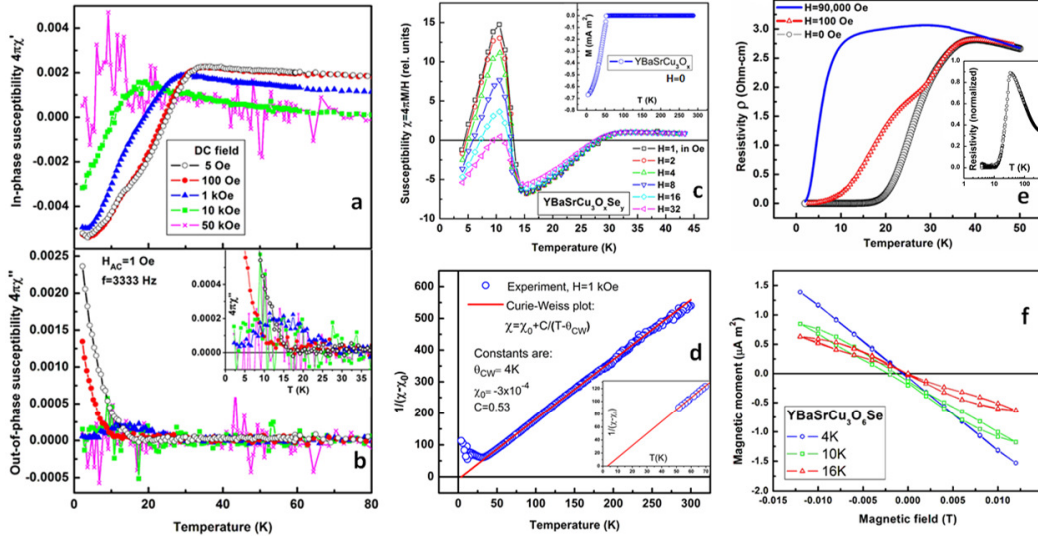


Figure 5: Sample properties in AC and DC magnetic fields. (a) Real and (b) imaginary parts of AC susceptibility (at  $f = 3333$  Hz and  $H_{AC} = 1$  Oe) are shown in various DC magnetic fields from 5 Oe to 50 kOe; inset in (b) illustrates the transition in greater detail. (c) Peculiar behavior (reentrant diamagnetism) of DC susceptibility with a strong paramagnetism above superconducting transition yielding the Curie-Weiss behavior; inset shows similar transition in a sample without Se. (d) Curie-Weiss behavior of experimental data on paramagnetism; inset shows linear extrapolation of experimental data in greater detail (circles correspond to average of 2 measurements). (e) Magnetoresistance in weak and strong magnetic fields. Inset shows noticeable re-entrant resistivity at  $T \lesssim 4$  K (see also [28]). (f)  $\mathbf{M}(\mathbf{H})$  at three characteristic temperatures.

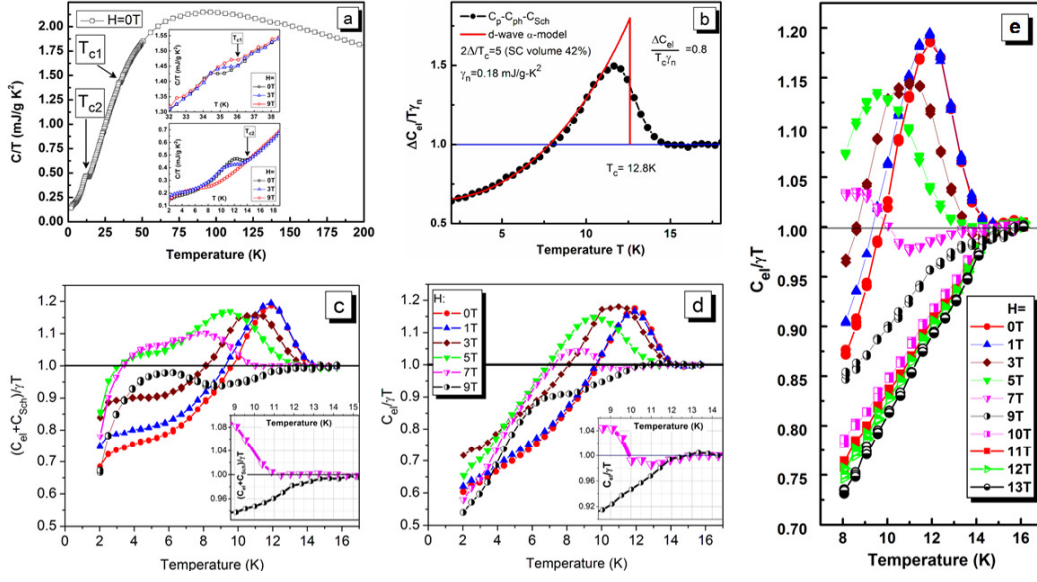


Figure 6: Heat capacity of the sample with the initially intended stoichiometry YBaSrCu<sub>3</sub>O<sub>6</sub>Se. (a) Two superconducting transitions (with  $T_{c1}$  and  $T_{c2}$ ) at  $H = 0$ ; insets illustrate details of these transitions in  $H = 0, 3$  and  $9$  T fields. (b) Modeling the transition of the major superconducting phase by the  $d$ -wave  $\alpha$ -model at  $H = 0$ . (c) Behavior of electronic specific heat with phonon contribution subtracted and Schottky anomaly present at bulk superconducting transition in different magnetic fields (the curve coding is similar to panel d). (d) The same behavior with the Schottky anomaly subtracted. Insets in panels (c) and (d) clarify the downturn at  $H = 9$  T. (e) Specific heat anomaly with increasing magnetic field (from 0 to 13 T) which reveals quantum criticality (explained in Discussion).

### 3. Discussion

#### 3.1. Diamagnetism

The AC susceptibility  $\chi'(T)$  (Fig. 5a) clearly indicates superconducting transition at about 30 K. More sophisticated is the behavior of the DC susceptibility (Fig. 5c) which reveals a peculiarity known as the Wohlleben effect (it will be discussed after Magnetoresistivity to better understand the material). Despite positiveness of DC susceptibility at certain temperature range, the dependence of magnetic moment vs. applied field,  $\mathbf{M}(\mathbf{H})$  (Fig. 5f), has negative derivatives at all temperatures below  $T_c$  – a feature which corresponds to the superconducting state.

#### 3.2. Magnetoresistivity

The second superconducting phase, which is responsible for the reentrant diamagnetism in Fig. 5c, is also noticeable in magnetoresistivity (Fig. 5e). This magnetoresistive behavior has a remarkable low-field feature ( $H = 0$  Oe and 100 Oe in Fig. 5e): above a certain temperature  $T > T_0$ ,  $\rho(T)(H = 0)$  and  $\rho(T)(H = 100)$  match with one another; however, at  $T < T_0$ , the higher-field curve delays with the transition to  $R = 0$  state. This is an unusual feature, caused, most likely, by the electron hopping. At lower temperatures and higher fields, the hopping through the grain boundary barrier becomes prohibited (or, alternatively, charge carrier trapping becomes more effective) yielding this observation. In stronger fields, the anomaly is gone and the  $\rho(T)$  behavior becomes typical, as Fig. 5e demonstrates at  $H = 90$  kOe. The divergent behavior of  $\chi''$  (Fig. 5b) is also most likely related to this mechanism: superconductivity in the intergranular areas disappears in higher fields, leaving only bulk intragranular effects both in  $\chi'$  and  $\chi''$ . Notably, at  $H = 50$  kOe, the fluctuations in the AC susceptibility become large and mask off the superconducting transition.

#### 3.3. Paramagnetism and Curie-Weiss behavior

The comparison of major curve in Fig. 5c with its inset indicates strong paramagnetism. Fitting the experimental data above  $T_{c1}$  in  $\text{YBa}_{2-x}\text{Sr}_x\text{Cu}_3\text{O}_{7-x}\text{Se}_x$  by the Curie-Weiss law  $\chi = \chi_0 + C/(T - \theta_{CW})$ , as shown in Fig. 5d, one can get the Curie-Weiss temperature  $\theta_{CW} \approx 4$  K at parameters  $\chi_0 \approx -3 \times 10^{-4}$  and  $C \approx 0.53$ . This implies [29, 30]:

$$\frac{\mu_{\text{eff}}}{\mu_B} \equiv p_{\text{eff}} = \sqrt{C} \frac{\sqrt{3k_B}}{\mu_B \sqrt{yN_A}} \approx 2.8 \sqrt{\frac{C}{y}} \approx 2.8 \quad (1)$$

where  $y$  is the actual Se content in  $\text{YBa}_{2-x}\text{Sr}_x\text{Cu}_3\text{O}_{7-x}\text{Se}_x$  (which, as follows from Table 1 and the XRD data, is about 0.5 – the number used in (1)). This means that per unit cell the average magnetic moment is  $\mu_{\text{eff}} \approx 1.5\mu_B$  (since only 50% of the superconducting phase possess Se). Also, one can estimate the total angular momentum  $J$  from the expression [30]:

$$\sqrt{J(J+1)} = p_{\text{eff}}/g \approx 1.4 \quad (2)$$

as  $J = 1$  (we adopted the electron gyromagnetic ratio  $g = 2$ ). Presence of positive Curie-Weiss temperature typically indicates ferromagnetism at  $T < \theta_{CW}$ . However, as follows from Fig. 5a, there is no ferromagnetic response visible in  $\chi'$  below  $T = 4$  K which is likely due to the competing superconducting order<sup>1</sup>. However, small ferromagnetic clusters are most likely existent, which can explain the small upturn (reentrant resistivity) visible at  $T \approx 4$  K in Fig. 5e inset. The upturn is also noticeable in  $\chi'$  (Fig. 5a) in small magnetic fields,  $H = 5$  Oe and  $H = 100$  Oe. With the field increase, at  $H = 0.1$  T, the upturn becomes less steep, and completely disappears in relatively strong fields ( $H = 1$  T and  $H = 5$  T). This can be explained by the orientation of magnetic moments of clusters, which makes the interaction of these moments with the external field less effective than for the random orientation. It points towards a preferable angle of orientation (easy axis) for the AC-field interaction with the magnetic moments, i.e., towards possible anisotropy. If this conclusion is correct, then much stronger upturns could appear at certain orientations of the applied magnetic field relative to the wave vector of the AC-probe field. Testing of this possible anisotropy could be considered as an interesting topic, though it is beyond the scope of the present article.

### 3.4. Wohleben effect

Numerous explanations have been suggested for understanding the mechanism of curves similar to ones shown Fig. 5c since the first discovery in granular high-temperature superconductors [31, 32], and later in many other superconducting objects including Al [33] and Nb [34] disks, Josephson junction systems [35, 36], In-Sn spheres [37], etc.

---

<sup>1</sup>This fact also indicates that the Curie-Weiss behavior is a property of the superconducting phase in our heterophase sample.

From a theoretical point of view, the magnetic moment (or magnetization  $\mathbf{M} = \mathbf{B} - \mathbf{H}$ ) of a superconductor is determined by a superfluid current  $\mathbf{j}_s$ :

$$\mathbf{M} = \frac{1}{2c} \int [\mathbf{j}_s \times \mathbf{r}] dV. \quad (3)$$

Thus, theoretical attempts to explain the effect ought to modify the traditional, Meissner-type behavior of these currents  $\mathbf{j}_s(\mathbf{r}, t)$  in a drastic manner to switch from the diamagnetic to the paramagnetic response. These attempts can principally be classified into two categories of models, the first of which is based on currents spontaneously flowing in superconductors in absence of an external field  $\mathbf{H}_{ext}$ . This field orients the randomly distributed local moments  $\mathbf{M}_i$  so that  $\langle \mathbf{M}_i \rangle > 0$ . The second category of models depends on more geometrically complex current patterns (in presence of  $\mathbf{H}_{ext}$ ) than envisioned by the ordinary theoretical approach. Because of the granular structure (Fig. 1), as well as the presence of effective magnetic moments in the lattice at low temperatures, the  $\pi$ -junction model [38] was a direct candidate to consider in our case. The likelihood of applicability of this model was further enhanced by the notion (discussed later in this article) that the  $d$ -wave superconductivity fits best to our heat capacity data (Fig. 6b). To judge the applicability of the  $\pi$ -junction model, we demolished one of our samples and ground it down to submicron sizes by milling it in a sapphire mortar. The powder was then thoroughly mixed with a glue, so as to eliminate intergranular couplings. Figure 7 compares the resultant DC susceptibility with that of the sample while still in a ceramic form.

The depth of the first diamagnetic transition (with an onset at 30-35 K), normalized to the paramagnetic signal, is drastically reduced. That is, for the same amount of contributing mass of  $\text{YBa}_{2-x}\text{Sr}_x\text{Cu}_3\text{O}_{7-x}\text{Se}_x$ , the diving amplitude of the first diamagnetic signal is much smaller (by a factor of 6 to 7). This can be explained by the idea that the first transition is related with the supercurrents flowing on the surface of the granules as well as the intergranular trajectories (the latter have been essentially destroyed by milling and subsequent application of the glue). As a result, the effective volume able to conduct screening superconducting currents is reduced. At the same time, the upturn amplitude is smaller only by a factor of two. Importantly, the temperature of upturn also did not change; most likely, this is because the second superconducting transition takes place inside of the granules and is not significantly impacted by the granular size reduction and the granules separation.

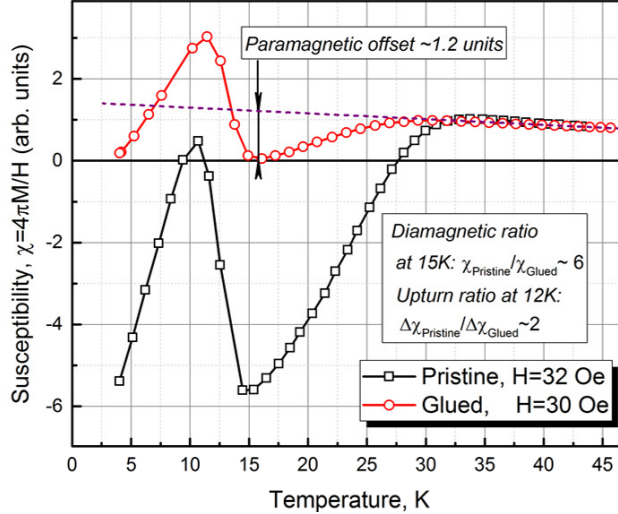


Figure 7: DC susceptibility measurements of pristine and powder-glued sample in  $H \sim 30$  Oe (similar results were obtained in  $H \sim 5$  Oe).

Overall, one can conclude that spontaneous currents due to the  $\pi$ -junctions, while being very elegant and possibly applicable to other systems, are not the cause of the Wohleben effect in our material. Flux compression looks more feasible. This model as formulated by Koshelev and Larkin [39], has been developed in detail by many works (see, e.g., [40] and Refs. therein). In granular superconductors, complete screening of applied external field  $\mathbf{H}_{ext}$  is not the only possibility, though it corresponds to the absolute minimum of Gibbs' energy. In some cases, it may happen that superconductivity first occurs on the granular surface. Then a flux may be trapped inside of a granule being confined by the superconducting shell layer. When the temperature is further reduced, the superconducting layer grows inwards, and a screening current of the same nature which initially occurred on the surface layer to screen-off the  $\mathbf{H}_{ext}$  rises around the trapped flux. From the topology it is clear that the direction of this current should be opposite to that of the surface one. In accordance to (3), this can revert the sign of magnetization, making it positive.

Using expressions (6) and (13) in the original work [39], one can obtain maximum paramagnetic to diamagnetic susceptibility ratio  $\sim 100\%$  for the the disk geometry. This value is very close to our data in Fig. 7 for the pristine sample.

One can expect the higher- $T_c$  phase to be on the surface of individual granules (with the lower Se content), while lower- $T_c$  phase (more rich with Se content) is inside the granules. This structural order is similar to the In-Sn-composition studied by Chu et al. [37]. In their study, the lower- $T_c$  superconducting volume was surrounded by a higher- $T_c$  phase, and the Wohleben effect was detected during the field cooling. From the point of view of the underlying physics, this structural order facilitates flux trapping and subsequent compression. Unsurprisingly, the resultant curves (Fig. 2 of Ref. [37]) resemble ours shown in Fig. 5c and Fig. 7.

### 3.5. Heat capacity anomaly

The heat capacity measurements and related results (Fig. 6) yield the major implications of our work, as will be clear from further discussions. The low-temperature superconducting phase, corresponding to  $T_{c2} = 12.8$  K, constitutes the majority. Thus, in our analysis of the heat capacity data, we will focus on this phase. Excluding the phonon and Schottky contributions (the details are provided in Methods), we find (Fig. 6b) that a rather good theoretical fit to our experimental data is possible within the  $d$ -wave  $\alpha$ -model (see, *e.g.*, [41, 42]). As follows from this fit, the superconducting phase content is about 42(*wt.*%) of the normal phase. This is not very far from the XRD results (30.6 *at.*% in Table II correspond to 44.4 *wt.*%).

Figure 6c,d contains a very unusual result. Namely, in the range  $H = 0-5$  T, with the  $\mathbf{H}$ -field increase, the transition temperature  $T_{c2}$  moves towards lower values and the ratio  $C_{el}(T)/\gamma T$  equals 1 at  $T > T_{c2}$  in accordance with expectations. However, for further increase of magnetic field (*i.e.*, at  $H = 7$  T and much more pronouncedly at  $H = 9$  T),  $C_{el}(T)/\gamma T$  exhibits a downturn at temperature  $T > T_{c2}$  (the reproducibility of this result has been confirmed on more than one sample; moreover, to eliminate possibility of data processing artifacts, we checked visibility of the downturn by comparing the 9 T  $C_p/T$  raw data with those in smaller fields: 7 T and below). The field 9T is still below  $H_{c2}$ , as follows from the resistivity curve in Fig. 5e,  $T_{c2} \sim 6$  K at  $H = 90,000$  Oe. At this temperature, the electronic heat capacity has a local maximum, Fig. 6c, which is still noticeable after the subtraction of the Schottky part (Fig. 6d). Remarkably, the subtraction of Schottky contribution does not significantly affect the onset temperature of the downturn. In absence of the downturn, the curve in case of  $H = 9$  T (as well as  $H = 7$  T) would have had the traditional shape (*i.e.*, similar to those at smaller values of  $H$ ).



Thus, we have an anomaly, which is shown in Fig. 6c,d, and is magnified in insets to them. Because of importance of this downturn (see the next subsection) we also performed measurements at higher fields  $H = 10$  T, 11 T, 12 T and 13 T. The results are summarized in Fig. 6e for more convincing evidence of the effect to be discussed in the next subsection.

Prior to proceeding to it, we will mention that the higher  $T_c$  transition, the  $T_{c1}$ -phase, is also visible in the top inset to Fig. 6a. As was mentioned at discussing the Wohleben effect, it may be just the crust contribution of the same bulk Phase 1 with less content of Se. Its field dependence contains another anomaly: the higher transition temperatures at higher fields. However, further discussion of this minor phase behavior is beyond the goals of this report.

### 3.6. Quantum criticality

Magnetic field-induced quantum phase transitions have been reported in heavy-fermion [43, 44, 45], iron-based [46, 47], and cuprate [48, 49, 50, 51] superconductors, as well as in metamagnets [52, 53], antiferromagnets [54, 55], and other systems [56]. Exploration of this important quantum-mechanical feature of superconducting state appears instrumental for deciphering the mechanism of high-temperature superconductivity.

In the case of quantum criticality, nearly degenerate ground states exist not only at very low (ideally zero) temperatures, but reveal themselves over a range of temperatures. Variation of external or internal parameters may cause border-crossing between the phases on phase diagrams. In the case of the second order phase transition, the system may possess a set of quantum critical points (QCPs) at certain values of tuning parameters [50]. It was recently recognized that the pseudogap (PG) phase of cuprates ends at QCP [20]. Moreover, the associated fluctuations can be involved in  $d$ -wave pairing and the anomalous scattering of charge carriers. Heat capacity measurements in the magnetic field [20] are instrumental for the observation of features relevant to quantum criticality. However, for cuprates, the critical fields are high, and the required values (e.g., 18 T in case of Eu-LSCO and Nd-LSCO [20], and 45 T in case of Tl-2201 [19]) exceed typically available limits of common laboratory apparatus. In case of Tl-2201, the heavily doped composition is chosen to reduce the value of  $T_c$  (and associated destructive magnetic field) from maximally available  $T_c = 93$  K down to 15 K. In cuprates, compositional modifications may serve as an alternative to

oxygen overdoping, thus reducing the values of required fields while keeping the typical features observable.

To understand the relationship of the heat capacity anomaly of the bulk phase with the quantum criticality, one should take into account that  $C_{el}(H)/T \equiv \gamma(H) \propto n(H)$ , where  $n$  is the charge carrier density. If at  $H > H_0$  (where  $H_0 \simeq 7$  T)  $n(T)$  decreases with the temperature then a non-Fermi liquid behavior takes place: in Fermi liquids,  $n$  (and  $\gamma$ ) does not depend on temperature. This kind of effect caused by application of strong magnetic fields was reported and explained by the fluctuating pair field and PG, which causes the downturn via the border crossing due to the doping [57, 58, 59]. In our case, the crossing of the border is due to the cooling in a high magnetic field. We suggest the explanation of its mechanism which is related with the existence of pair density wave (PDW) [60], and the charge density waves (CDW) as its consequence [61]. The emergence of CDW requires the doping range  $0.08 < p_{CDW} < 0.16$ . Within this doping level, in high-enough magnetic fields (i.e., at  $H > H_0$ ), the CDW border crossing occurs as soon as the temperature drops below a certain value. In pure YBCO, this occurs at  $T < 20$  K in  $H = 50$  T [62, 63]. During this process, the re-arrangement of phases inherent to cuprate superconductors relative to the QCPs on the field-doping phase diagram takes place.

Appearance of CDW reduces the density of charge carriers. This is associated with the creation of electron pockets<sup>2</sup> on Fermi arcs, and this mechanism reveals itself in Hall [62, 63], Nernst [64] and Seebeck [65, 64] effects. In particular, the Hall coefficient  $R_H$  for  $H > H_0$ , decreases from its zero value and becomes negative at low-enough temperatures. The increase of the absolute value of  $R_H \propto 1/n$  corresponds to the decrease in charge carrier density  $n$  (see [62]).

An alternative explanation involves the incommensurate SDW [66] rather than CDW. The latter will be prohibited if  $p < 0.08$ . If Se, like O, provides doping to the CuO conductivity layer, the doping parameter  $p$  (i.e., the number of holes per Cu) may be estimated by the universal trend reported

---

<sup>2</sup>Interestingly, in addition to the electron pockets on the Fermi arcs, experimental evidence is obtained in favor of two nearby hole-type pockets [64], so that the electronic specific heat is a combination of three contributions, of which the hole pockets contribute about 17.3% each to 65.4% of the electron pocket contribution. Unlike the Hall effect, these electron and hole pocket charge carriers contribute constructively to the specific heat thus increasing the overall effect of the magnetic field.

in Ref. [67]:

$$\frac{T_c}{T_c^{\max}} = 1 - 82.6(0.16 - p)^2. \quad (4)$$

Here,  $T_c^{\max}$  is the value of  $T_c$  at the optimal doping for our material. The CDW condition  $0.08 < p < 0.16$  [68, 69] infers a range of possible values for  $T_c^{\max}$ :  $12.8 \text{ K} < T_c^{\max} < 27.2 \text{ K}$ . The inhomogeneity-caused broad range of  $T_c$  values visible in Fig. 6b allows the emergence of quantum criticality at 15 K which is in accordance with the downturn temperature  $\sim 15 \text{ K}$  of 9 T and higher field-caused QCP in Fig. 6c-e. As known for HTSC cuprates [57, 58, 59], at  $T = 0$ ,  $p_{PG} = 0.19$ . Corresponding value of  $T_c^{\max}$  from (4) is then  $\sim 14 \text{ K}$ , which, within the experimental inaccuracy, is close to the declared 15 K. The fact that the QCP observational temperature is dramatically higher than  $T = 0$  in both competing cases is not surprising in view of the well-established “fanning out” effect [70] reported previously [50, 62] in HTSC cuprates.

For pure single-crystal measurements, involvement of quantum criticalities yields peculiarities in resistivity  $\rho$ . For example, a drastic upturn takes place at PG when superconductivity is fully suppressed [58] by  $H > H_{c2}$ : the upturn starts gradually much below the pseudogap opening temperature  $T_\rho$ . Also, two competing mechanisms (reduction of inelastic scattering and reduction of charge carrier density) may coexist, so the resultant behavior of  $\rho(T)$  may be both upturn and downturn. In our case,  $H_{max} = 9 \text{ T} < H_{c2}$ . Additionally, in our case, we have the second, higher- $T_c$  phase which can mask-off any gradual changes in  $\rho$ ; moreover, as follows from the inset in Fig. 5e, granular crusts are causing semiconductor-type temperature behavior of  $\rho(T)$  above  $T_{c1}$  thus obscuring involvement of arguments related with the reported behavior of resistivity. Having single crystals of this composition where the value of  $p$  depends on Se concentration  $y$  would further facilitate research in these cuprates. In particular, one can explore oscillations of the Seebeck and Nernst coefficient (see Fig 2 in [64]) and other effects caused by quantum criticality in much more accessible magnetic fields. In the course of our research the doping parameter was kept constant; principally, additional opportunities may come from variation of Se concentration as a QCP tuning parameter.

In general, simultaneous doping of mother substance  $\text{YBa}_2\text{Cu}_3\text{O}_7$  by Sr and Se provides more flexibility in modifying this remarkable system than mono-element substitution. The price to pay for this flexibility is multiphase

nature of the sample. However, after this study, one can try to target more precisely the composition  $\text{YBa}_{1.4}\text{Sr}_{0.6}\text{Cu}_3\text{O}_6\text{Se}_{0.51}$  with the adjusted initial stoichiometry - a fair task for future experimental research. Also, explaining why its properties are drastically different from the isomorphous  $\text{YBa}_2\text{Cu}_3\text{O}_{6.51}$  would be very challenging for the theory.

#### 4. Conclusions

In summary, we obtained striking anomalies delivered by simultaneous double substitution of Ba by Sr and O by Se in a pristine  $\text{YBa}_2\text{Cu}_3\text{O}_7$  superconductor. Simultaneous application of EDX and EBSD proved that Se enters into the crystal lattice of the superconducting phase of polycrystalline heterogeneous material. Two superconducting transitions are revealed. One phase, with  $T_{c1} \approx 35$  K, and the second one, with lower  $T_{c2} \approx 13$  K. The latter phase,  $\text{YBa}_{1.4}\text{Sr}_{0.6}\text{Cu}_3\text{O}_6\text{Se}_{0.51}$  constitutes the majority of the superconductor. The second transition, most likely is caused by the granular surface of the same substance with less amount of Se on the surface of granules. Heat capacity explorations proved the  $d$ -wave nature of the main phase, as well as the existence of electronic Schottky anomaly in it. Susceptibility measurements revealed magnetic clusters below the Curie temperature  $\approx 4$  K. These magnetic moments, related with Se ligands of Cu, are reported for the first time. In view of provided XRD information on crystallographic positions of elements in superconducting phase, fruitful theoretical exploration should become possible, as it happened with As vacancies in  $\text{LaO}_{0.9}\text{F}_{0.1}\text{FeAs}_{1-\delta}$  ( $\delta \approx 0.06$ ) [30]. The most important finding in our report is related with the anomaly in the heat capacity data in moderately strong (7 – 9 T) magnetic fields. Various scenarios related with the competing PDW and PG QC border crossing can explain the obtained effect. Further experimental work and theoretical analysis on coexistence of PDW/PG and superconductivity will be easier in  $\text{YBa}_{2-x}\text{Sr}_x\text{Cu}_3\text{O}_{7-x}\text{Se}_x$  than in pure YBCO due to the less stringent magnetic field requirement, preferably on single-crystalline or single-phase samples, and could reveal more understanding of interrelationship between the physical effects reported here and the mechanism of superconductivity in cuprates.

## 5. Methods

### 5.1. Materials preparation

Polycrystalline samples were prepared via standard solid-state synthesis routes. Powders of  $Y_2O_3$ ,  $SrCO_3$ ,  $BaCO_3$ ,  $CuO$  and  $SrSe$  were mixed in stoichiometric proportions to form, after calcination, initial composition  $YBa_{2-x}Sr_xCu_3O_{7-x}Se_x$  ( $x = 0, 0.5, 0.75, 1$ ). After thorough mixing (hand mixing in sapphire mortar for 40 – 50 min per 400 mg of total constituents, or, alternatively, combination of initial 10 min of hand mixing with  $4 \times 5$  min of mechanical mill mixing (in plastic vials with agate balls), the mixture was calcined at  $900^\circ C$  for 100 min in KSL-1100 furnace in air, then re-ground, milled again, and pelletized for the second thermal treatment, which was done at  $950^\circ C$  for 30 min. It was then continued at  $650^\circ C$  for 80 min. Though the elemental composition of synthesized samples may be different from the initial targeted stoichiometry, we still call the resultant composition as  $YBa_{2-x}Sr_xCu_3O_{7-x}Se_x$ . Several pellets were prepared, with diameter 4 mm, height 1.5 mm for resistivity and magnetic measurements, and with diameter 1.5 mm and height 2 mm for heat capacity measurements. The most interesting features were discovered in case of the initial stoichiometry with  $x = 1$ , so only this case is being discussed in this report.

### 5.2. Compositional Analysis

For quantitative EDX analysis, ion milling was performed. The sample surface was polished so as to avoid the undesired self-absorption which affects proper outcome for light elements (O and Se in particular). For this task, the fine-ground powder was suspended in isopropyl alcohol, and dropped into a gap between a stainless steel holder and aluminum foil touching it as shown in Fig. 8a.

The cutting by ion knife was arranged in Hitachi Broad Ion Milling System, IM4000Plus, which cut the structure horizontally, providing a polished surface for microanalysis (Fig. 8b). The SEM EDX data were acquired from a large surface area, and the revealed composition closely resembled the initial chosen stoichiometry of the specimen: the data reflected in Table 1 (last line) confirm that a rather significant amount of Se remains in the material.

A Hitachi SU5000 variable pressure field emission scanning electron microscope (VP-FESEM) with Oxford Instruments EDX and EBSD under AZtec software was used for simultaneous EDX/EBSD analysis with electron beam focal diameter  $\sim 1 - 10$  nm which is suitable for the proposed

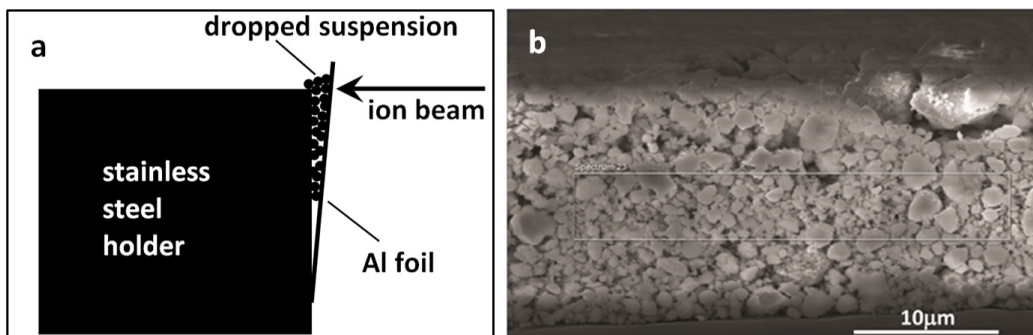


Figure 8: Polishing the powder via ion-milling. (a) Arrangement for cutting by ion knife. (b) Surface of powder prepared for EDX after the ion cutting.

Table 4: Parameters of the powder diffraction experiment

Diffractometer	Rigaku MiniFlex 600
Radiation	Cu-K $\alpha$
Wavelength, Å	1.540593
Detector name	D/teX Ultra2
Detector type	point
Scan range, deg	10.0 - 110.0
Scan step, deg	0.005
Scan speed, deg/ min	1.0
Incident slit, type, deg	Soller slit, 5.0
Receiving slit, type, deg	Soller slit, 5.0

task since it is comparable with the size of the lattice cell. During this stage of exploration, no ion polishing was applied. Instead, in order to avoid self-absorption, we changed the incidence angle of the electron beam until a Kikuchi pattern appeared (Fig. 3b) for identifying the crystalline structure (Fig. 3c). We then determined the chemical composition via EDX (Fig. 3d) at the same region of interest.

### 5.3. X-ray diffraction studies

Diffraction experiments were performed with polycrystalline samples in accordance with the data given in Table 4.

Qualitative phase analysis was performed with the code HighScore Plus 3.0e [71]. Heterophase nature of the sample was revealed and for the explanation of all detected peaks, five phases have been involved.

Refinement of structural models of these phases was performed using Jana2006 software [72]. Complex heterophase content of sample yielded strong correlations between the refining parameters of the models. For the reduction of the influence of these correlations on the results of our analysis we used various methods, the main of which was cyclic combination of Rietveld's approach [73, 74] and Le Bail's approach [75] which significantly increased the stability of the refinement and much improved the fit. The complexity of the problem arose from the small amount of Se dopant which cannot provide strong response at the scattering of X-rays. Nevertheless, because of the achieved high level of relative precision, we were able to detect the difference between the three cases shown in Table 5.

Table 5: Refinement comparison for three models of Se location in the structure  $\text{YBa}_{1.4}\text{Sr}_{0.6}\text{Cu}_3\text{O}_6\text{Se}_{0.51}$

No	Model	$R1, \%$	$w, \%$	$\Delta\rho_{\text{max}}, e/\text{\AA}^3$	$\Delta\rho_{\text{min}}, e/\text{\AA}^3$
1 [21]	Additional O positions: O4( $x,0.5,0$ ) and O5( $0.5,0,0$ ); Se is absent in the structure <sup>a</sup>	0.98	0.90	+0.30	-0.48
2 [15]	Se partially replaces Y <sup>b</sup>	1.09	0.93	+0.36	-0.54
3 Our model	Se is localized at positions Se4( $x,0.5,0$ ) and Se5( $0.5,0,0$ ) <sup>c</sup>	0.87	0.73	+0.17	-0.30

<sup>a</sup> At full matrix refinement, because of correlational shift, the  $x$ -coordinate of position O4 is unrealistic.

<sup>b</sup> Such heterovalent substitution looks improbably; we considered this opportunity for the test of literature data. It worsens refinement parameters; the results are unrealistic.

<sup>c</sup> In this model, the full matrix refinement is possible; moreover, with the simultaneous refinement of populations and ADP for incompletely occupied or shifted positions.



Table 6: Details of structural refinement for  $\text{YBa}_{1.4}\text{Sr}_{0.6}\text{Cu}_3\text{O}_6\text{Se}_{0.51}$  crystalline phase

Temperature (K)	294
Crystal system	Orthorhombic
space group, $Z$	$Pmmm$ , 1
$a, b, c$ (Å)	3.84359(4), 3.83295(6), 11.47722(17)
$V$ (Å <sup>3</sup> )	169.092(4)
$Dx$ (g/cm <sup>3</sup> )	6.8015
$\mu$ (mm <sup>-1</sup> )	83.432
<i>Profile fit</i>	
Profile function	Pseudo-Voigt
No. of measured points	20001
$R_p$ , %	1.32
$wR_p$ , %	1.92
$GOF$ (S)	3.14
<i>Structure model fit</i>	
Refinement based on $F$ with a weighting scheme	$1/\sigma^2(F)$
No of Bragg reflections, parameters	152, 18
$R1$ , %	0.87
$wR$ , %	0.73
$\Delta\rho_{\max}/\Delta\rho_{\min}$ , e/Å <sup>3</sup>	+0.17 / -0.30
Software	HighScore Plus, Jana2006

These model results were compared against each other using the criterion of refinement stability and factors  $R1$  and  $wR$ . It turned out that for the localization of dopant atoms, the extrema of difference Fourier synthesis,  $\Delta\rho_{\max}/\Delta\rho_{\min}$  are more informative. This criterion is usually considered as the second main one for the refinement of structural models. The main superconducting phase was determined in Model 3 with significant reduction of  $R$ -factors for the same number of Bragg reflections (152) and refinement parameters (18) as with Models 1 and 2. The highest residual peaks of difference electronic density are localized near heavy cations. The details of the refinement are given in Table 6.

#### 5.4. Processing of heat capacity data

Assuming that (at low temperatures) the heat capacity in our samples has three major contributions, we can write

$$C(T) = C_{el}(T) + C_{ph}(T) + C_{Sch}(T), \quad (5)$$

where  $C_{el}(T)$  stands for the electronic contribution containing both the normal part  $\gamma T$  and the superconductor part,  $C_{ph}(T) = \beta T^3$  characterizes the

phonon contribution, and the last term is the Schottky anomaly, which, in case of the simplest two-level gap  $\Delta_{tl}$  can be represented as [76]

$$C_{Sch}(T) = R \left( \frac{\Delta_{tl}}{T} \right)^2 \frac{\exp(\Delta_{tl}/T)}{[1 + \exp(\Delta_{tl}/T)]^2}. \quad (6)$$

At the first stage, the phonon contribution was subtracted from the experimental data<sup>3</sup>. For that task,  $C(T)/T$  was plotted as a function of  $T^2$ . Since the Schottky contribution (6) is negligible (exponentially small) at  $T = 0$ , the inclination of  $C(T)/T$  near the origin of coordinates provides the value of  $\beta$  (in our case,  $\beta \approx 0.04$  (Fig. 6)). Also, the value of  $C(T)/T$  at  $T = 0$  equals  $\gamma$ . After the subtraction of phonon contribution, the deviation from typical electronic contribution of superconducting state becomes evident (cf. Fig. 6c-e).

The characteristic superconducting behavior is restored by the subtraction of the Schottky contribution (6). After these operations are performed, one can make the second iteration, which involves computer coding. In the first step in this code, the Schottky curve is subtracted from the experimental data in accordance to (5) while allowing the opportunity to vary the gap  $\Delta_{tl}$  and the prefactor  $R$  around the values obtained at the initial stage. Then, the code computes the corresponding values of  $\beta$  and  $\gamma$ . These values are not too far from the ones determined at the initial stage, but performing the iteration is useful for ensuring better data processing for further analysis. The curves in Fig. 6d were obtained via this procedure from Fig. 6c.

For the theoretical modeling (Fig. 6b), we used the standard expression for heat capacity [42], which, in dimensionless form, can be represented as:

$$\frac{C_{el}(t)}{T_c} = \frac{1}{4t^2} \int_0^{2\pi} d\varphi \int_0^\pi d\theta \sin \theta \int_{-\infty}^{\infty} dx \frac{x^2 + \delta(t)^2 - t\delta(t) [d\delta(t)/dt]}{\cosh^2 \left[ \sqrt{x^2 + \delta(t)^2} / (2t) \right]}, \quad (7)$$

---

<sup>3</sup>It is worth to mention that our heterophase substance contains “parasitic” contributions to the heat capacity of the superconducting Phase 1. At  $T = 15$  K, the  $C/T$  of major phases 2 – 4 are (in mJ/(K<sup>2</sup> g-at) units):  $\sim 1$  for BaSeO<sub>4</sub> [77],  $\sim 0.52$  for Y<sub>2</sub>Cu<sub>2</sub>O<sub>5</sub> [78], and  $\sim 20$  for Y<sub>2</sub>BaCuO<sub>5</sub> [79]. These exceed the contribution of the superconducting phase (Fig. 5a). However, their contribution is mainly phononic in origin, and subtraction of  $\beta T^2$  from  $C/T$  extinguishes it as well as the contribution of the minor phase BaCu(SeO<sub>3</sub>)<sub>2</sub>.

where:  $T/T_c \equiv t$ ;  $\xi/T_c \equiv x$ ;  $\Delta(T)/T_c \equiv \delta(t)$ ;  $\varepsilon/T_c \equiv \sqrt{\xi^2 + \Delta^2}/T_c = \sqrt{x^2 + \delta^2}$ . In (7), one should substitute the value of the order parameter (the gap), which has the form  $\Delta = \Delta_0$  for isotropic  $s$ -wave and  $\Delta = \Delta_0 \cos n\phi$  for line nodes ( $n = 2$  for  $d$ -wave  $\alpha$ -model) [41, 80]. The temperature dependence of  $\Delta(T)$  was defined via the analytical expression [81] for BCS solution:

$$\begin{aligned} \frac{\Delta}{\Delta(0)} &= \sqrt{1-t}(0.9663 + 0.7733t), \text{ if } t > 0.33 \\ &= 1 \text{ otherwise.} \end{aligned} \quad (8)$$

Computation of  $C_{el}(T)/T$  based on (7) and (8) was performed numerically both for the  $s$ -wave and the  $d$ -wave cases. The best result is shown in the Fig. 3b. It corresponds to the Schottky parameters  $\Delta_{tl} = 10.5 \pm 0.1$  K,  $R = 0.31 \pm 0.01$ . This value of  $\Delta_{tl}$  is close the Schottky gaps in YBCO materials [82]. This matching justifies application of the simple relation (6) instead of more sophisticated expression [83]:

$$C_{Sch} = R \frac{dE_{Sch}}{dT}, \quad (9)$$

where

$$E_{Sch} = \sum E_i \exp(-E_i/T) / \sum \exp(-E_i/T), \quad (10)$$

and  $E_i = g\mu_B M_J H_{eff}$  where  $M_J = \{-S, -S + 1, \dots, S - 1, S\}_i$ ,  $H_{eff} = \sqrt{H_0^2 + H_{ext}^2}$  where  $H_0$  and  $H_{ext}$  are the internal and external field values. In the case of double levels ( $S = 1/2$ ), (9) transforms into (6) and the value of  $\Delta_{tl}$  is expressed by the external and the internal fields  $H_{ext}$  and  $H_0$ . In the case of  $S = 5/2$  (which corresponds to the 2+ states of copper ions), we obtained that the same level of matching as in Fig. 6b is possible at somewhat lower values of  $H_0$ . Whichever case is more relevant to our material requires further analysis. Also, the physical cause of the Schottky anomaly in our case remains uncertain: in addition to scattering on magnetic clusters, the scattering on minor amount of rare earth impurities [82] is an alternative. However, the details of Schottky anomaly are not significant for our main results, and we will not dwell more on this topic.

## 6. Data availability

The data that support the findings of this study are available from the corresponding author upon reasonable request.

## 7. Code availability

Full code that support the findings of this study are available from the corresponding author upon reasonable request.

## 8. Acknowledgments

A.D. acknowledges support by the Ministry of Science and Higher Education of the Russian Federation within the State assignment FSRC "Crystallography and Photonics" RAS in part of X-rays diffraction study. The work of the Chapman U. research team is supported by the US Office of Naval Research Grants No. N00014-21-1-2879 and N00014-20-1-2442. We are grateful to E. Vinogradova for assistance.

## 9. Author contributions

A.G., V.N., V.G. and S.N. designed research; A.G., V.G., V.N., J.K., A.M., J.C., I.P, R.D., S.T., T.H. and S.C. performed research, A.G., V.N., V.G., A.D., R.D., S.T. and S.C. analyzed data; and A.G., V.G., A.D., R.D., S.T. and S.C. wrote the paper.

## References

- [1] H. Kamerlingh Onnes, Further experiments with liquid helium. C. On the change of electric resistance of pure metals at very low temperatures etc. IV. The resistance of pure mercury at helium temperatures, Koninklijke Nederlandse Akademie van Wetenschappen Proceedings Series B Physical Sciences 13 (1910) 1274–1276.
- [2] J. Matricon, G. Waysand, The Cold Wars: A History of Superconductivity, The Cold Wars: A History of Superconductivity, Rutgers University Press, 2003.
- [3] J. G. Bednorz, K. A. Müller, Possible high  $T_c$  superconductivity in the Ba–La–Cu–O system, Zeitschrift für Physik B Condensed Matter 64 (2) (1986) 189–193. doi:10.1007/BF01303701.
- [4] M. K. Wu, J. R. Ashburn, C. J. Torng, P. H. Hor, R. L. Meng, L. Gao, Z. J. Huang, Y. Q. Wang, C. W. Chu, Superconductivity at 93 K in a new mixed-phase Y-Ba-Cu-O compound system at ambient pressure, Phys. Rev. Lett. 58 (1987) 908–910. doi:10.1103/PhysRevLett.58.908.

- [5] Z. Z. Sheng, A. M. Hermann, Bulk superconductivity at 120 K in the Tl–Ca/Ba–Cu–O system, *Nature* 332 (6160) (1988) 138–139. doi:10.1038/332138a0.
- [6] A. Schilling, M. Cantoni, J. D. Guo, H. R. Ott, Superconductivity above 130 K in the Hg–Ba–Ca–Cu–O system, *Nature* 363 (6424) (1993) 56–58. doi:10.1038/363056a0.
- [7] H. Maeda, Y. Tanaka, M. Fukutomi, T. Asano, A New High-Tc Oxide Superconductor without a Rare Earth Element, *Japanese Journal of Applied Physics* 27 (2A) (1988) L209. doi:10.1143/JJAP.27.L209.
- [8] C.-H. Yee, G. Kotliar, Tuning the charge-transfer energy in hole-doped cuprates, *Phys. Rev. B* 89 (2014) 094517.
- [9] C.-H. Yee, T. Birol, G. Kotliar, Guided design of copper oxysulfide superconductors, *EPL (Europhysics Letters)* 111 (1) (2015) 17002. doi:10.1209/0295-5075/111/17002.
- [10] L. Palhan, A. Brokman, I. Felner, M. Brettschneider, Y. Yacoby, M. Weger, Does sulfur replace oxygen in the superconducting  $\text{YBa}_2\text{Cu}_3\text{O}_{6\text{S}}$  phase?, *Solid State Communications* 68 (3) (1988) 313 – 317.
- [11] R. Cloots, A. Rulmont, P. Godelaine, C. Hannay, H. Vanderschueren, M. Ausloos, Sulphur substitution for oxygen in  $\text{YBa}_2\text{Cu}_3\text{O}_7$  ceramics, *Solid State Communications* 79 (7) (1991) 615 – 619.
- [12] S. Cooke, J. Allison, R. Woods, High-temperature resistivity measurements of  $\text{YBa}_2\text{Cu}_3\text{O}_{7-\delta}$  doped with sulphur, *Solid State Communications* 112 (4) (1999) 229 – 233.
- [13] R. Gagnon, P. Fournier, M. Aubin, A. H. O’Reilly, J. E. Greedan, Superconductivity in sulfur-containing *R*-Ba-Cu-O compounds, *Phys. Rev. B* 39 (1989) 11498–11502. doi:10.1103/PhysRevB.39.11498.
- [14] S. Kambe, M. Kawai, Effect of S, Se and Te Addition on the Superconductive Properties of  $\text{Ba}_2\text{YCu}_3\text{O}_{7-y}$ , *Japanese Journal of Applied Physics* 27 (Part 2, No. 12) (1988) L2342–L2344. doi:10.1143/jjap.27.12342.

- [15] Z. D. Yakinci, D. M. Gokhfeld, E. Altin, F. Kurt, S. Altin, S. Demirel, M. A. Aksan, M. E. Yakinci, Jc enhancement and flux pinning of Se substituted YBCO compound, *Journal of Materials Science: Materials in Electronics* 24 (12) (2013) 4790–4797. doi:10.1007/s10854-013-1476-8.
- [16] A. Slebarski, A. Chelkowski, J. Jelonek, A. Kasprzyk, Effect of substitution of O by Se on the superconductivity of  $\text{YBa}_2\text{Cu}_3\text{O}_7$ , *Solid State Communications* 73 (7) (1990) 515 – 517.
- [17] I. Felner, I. Nowik, Y. Yeshurun, Effects of substitution of O by S and Cu by Fe on superconductivity in  $\text{YBa}_2\text{Cu}_3\text{O}_7$ , *Phys. Rev. B* 36 (1987) 3923–3925.
- [18] I. Felner, B. Barbara, Effect of sulfur on the superconductivity of  $\text{RBa}_2\text{Cu}_3\text{O}_7$ , *Phys. Rev. B* 37 (1988) 5820–5823.
- [19] T. Shibauchi, L. Krusin-Elbaum, M. Hasegawa, Y. Kasahara, R. Okazaki, Y. Matsuda, Field-induced quantum critical route to a Fermi liquid in high-temperature superconductors, *Proceedings of the National Academy of Sciences* 105 (20) (2008) 7120–7123. doi:10.1073/pnas.0712292105.
- [20] B. Michon, C. Girod, S. Badoux, J. Kačmarčík, Q. Ma, M. Dragomir, H. A. Dabkowska, B. D. Gaulin, J.-S. Zhou, S. Pyon, T. Takayama, H. Takagi, S. Verret, N. Doiron-Leyraud, C. Marcenat, L. Taillefer, T. Klein, Thermodynamic signatures of quantum criticality in cuprate superconductors, *Nature* 567 (7747) (2019) 218–222. doi:10.1038/s41586-019-0932-x.
- [21] F. Licci, A. Gauzzi, M. Marezio, G. P. Radaelli, R. Masini, C. Chaillout-Bougerol, Structural and electronic effects of Sr substitution for Ba in  $\text{Y}(\text{Ba}_{1-x}\text{Sr}_x)_2\text{Cu}_3\text{O}_w$  at varying w, *Phys. Rev. B* 58 (1998) 15208–15217. doi:10.1103/PhysRevB.58.15208.
- [22] C. Pistorius, M. Pistorius, Lattice constants and thermal-expansion properties of the chromates and selenates of lead, strontium and barium, *Zeitschrift für Kristallographie* 117 (4) (1962) 259–272.
- [23] R. D. Adams, J. A. Estrada, T. Datta, Crystal structure analysis of  $\text{Y}_2\text{Cu}_2\text{O}_5$ , *Journal of Superconductivity* 5 (1) (1992) 33–38.

- [24] J. Aride, S. Flandrois, M. Taibi, A. Boukhari, M. Drillon, J. Soubeyrou, New investigation on magnetic and neutron diffraction properties of  $\text{Y}_2\text{Cu}_2\text{O}_5$  and related oxides, *Solid State Communications* 72 (5) (1989) 459–463.
- [25] R. Hsu, E. N. Maslen, N. Ishizawa, A synchrotron X-ray study of the electron density in  $\text{Y}_2\text{BaCuO}_5$ , *Acta Crystallographica Section B* 52 (4) (1996) 569–575. doi:10.1107/S0108768196000250.
- [26] H. Effenberger, Three modifications of  $\text{BaCu}(\text{SeO}_3)_2$  and the compound  $\text{SrCu}(\text{SeO}_3)_2$ : Preparation and crystal structure determination, *Journal of Solid State Chemistry* 70 (2) (1987) 303 – 312. doi:https://doi.org/10.1016/0022-4596(87)90069-7.
- [27] B. H. Toby, R factors in Rietveld analysis: How good is good enough?, *Powder Diffraction* 21 (1) (2006) 67–70. doi:10.1154/1.2179804.
- [28] A. Gulian, V. Nikoghosyan, J. Tollaksen, V. Vardanyan, A. Kuzanyan, Current-biased Transition-edge Sensors Based on Re-entrant Superconductors, *Physics Procedia* 67 (2015) 834 – 839, proceedings of the 25th International Cryogenic Engineering Conference and International Cryogenic Materials Conference 2014.
- [29] R. A. Levy, *Principles of Solid State Physics*, Academic Press, New York, 1968.
- [30] V. Grinenko, K. Kikoin, S.-L. Drechsler, G. Fuchs, K. Nenkov, S. Wurmehl, F. Hammerath, G. Lang, H.-J. Grafe, B. Holzapfel, J. van den Brink, B. Büchner, L. Schultz, As vacancies, local moments, and Pauli limiting in  $\text{LaFeAs}_{1-\delta}\text{O}_{0.9}\text{F}_{0.1}$  superconductors, *Phys. Rev. B* 84 (2011) 134516. doi:10.1103/PhysRevB.84.134516.
- [31] Y. Yeshurun, I. Felner, H. Sompolinsky, Magnetic properties of a high- $T_c$  superconductor  $\text{YBa}_2\text{Cu}_3\text{O}_7$ : Reentry-like features, paramagnetism, and glassy behavior, *Phys. Rev. B* 36 (1987) 840–842. doi:10.1103/PhysRevB.36.840.
- [32] P. Svedlindh, K. Niskanen, P. Norling, P. Nordblad, L. Lundgren, B. Lönnberg, T. Lundström, Anti-Meissner effect in the  $\text{BiSrCaCuO}$ -system, *Physica C: Superconductivity and its Applications* 162-164

- (1989) 1365 – 1366. doi:[https://doi.org/10.1016/0921-4534\(89\)90735-1](https://doi.org/10.1016/0921-4534(89)90735-1).
- [33] A. K. Geim, S. V. Dubonos, J. G. S. Lok, M. Henini, J. C. Maan, Paramagnetic Meissner effect in small superconductors, *Nature* 396 (6707) (1998) 144–146. doi:[10.1038/24110](https://doi.org/10.1038/24110).
- [34] J. J. Palacios, Vortex matter in superconducting mesoscopic disks: Structure, magnetization, and phase transitions, *Phys. Rev. B* 58 (1998) R5948–R5951. doi:[10.1103/PhysRevB.58.R5948](https://doi.org/10.1103/PhysRevB.58.R5948).
- [35] F. M. Araujo-Moreira, P. Barbara, A. B. Cawthorne, C. J. Lobb, Reentrant ac Magnetic Susceptibility in Josephson-Junction Arrays, *Phys. Rev. Lett.* 78 (1997) 4625–4628. doi:[10.1103/PhysRevLett.78.4625](https://doi.org/10.1103/PhysRevLett.78.4625).
- [36] P. Barbara, F. M. Araujo-Moreira, A. B. Cawthorne, C. J. Lobb, Reentrant ac magnetic susceptibility in Josephson-junction arrays: An alternative explanation for the paramagnetic Meissner effect, *Phys. Rev. B* 60 (1999) 7489–7495. doi:[10.1103/PhysRevB.60.7489](https://doi.org/10.1103/PhysRevB.60.7489).
- [37] S. Chu, A. J. Schwartz, T. B. Massalski, D. E. Laughlin, Extrinsic paramagnetic Meissner effect in multiphase indium-tin alloys, *Applied Physics Letters* 89 (11) (2006) 111903. doi:[10.1063/1.2352805](https://doi.org/10.1063/1.2352805).
- [38] M. Sigrist, T. M. Rice, Unusual paramagnetic phenomena in granular high-temperature superconductors—A consequence of  $d$ - wave pairing?, *Rev. Mod. Phys.* 67 (1995) 503–513. doi:[10.1103/RevModPhys.67.503](https://doi.org/10.1103/RevModPhys.67.503).
- [39] A. E. Koshelev, A. I. Larkin, Paramagnetic moment in field-cooled superconducting plates: Paramagnetic Meissner effect, *Phys. Rev. B* 52 (1995) 13559–13562. doi:[10.1103/PhysRevB.52.13559](https://doi.org/10.1103/PhysRevB.52.13559).
- [40] G. F. Zharkov, Paramagnetic Meissner effect in superconductors from self-consistent solution of Ginzburg-Landau equations, *Phys. Rev. B* 63 (2001) 214502. doi:[10.1103/PhysRevB.63.214502](https://doi.org/10.1103/PhysRevB.63.214502).
- [41] D. C. Johnston, Elaboration of the  $\alpha$ -model derived from the BCS theory of superconductivity, *Superconductor Science and Technology* 26 (11) (2013) 115011. doi:[10.1088/0953-2048/26/11/115011](https://doi.org/10.1088/0953-2048/26/11/115011).



- [42] C. L. Huang, J.-Y. Lin, C. P. Sun, T. K. Lee, J. D. Kim, E. M. Choi, S. I. Lee, H. D. Yang, Comparative analysis of specific heat of  $\text{YNi}_2\text{B}_2\text{C}$  using nodal and two-gap models, *Phys. Rev. B* 73 (2006) 012502. doi:10.1103/PhysRevB.73.012502.
- [43] J. Custers, P. Gegenwart, H. Wilhelm, K. Neumaier, Y. Tokiwa, O. Trovarelli, C. Geibel, F. Steglich, C. Pépin, P. Coleman, The break-up of heavy electrons at a quantum critical point, *Nature* 424 (6948) (2003) 524–527. doi:10.1038/nature01774.
- [44] A. Bianchi, R. Movshovich, I. Vekhter, P. G. Pagliuso, J. L. Sarrao, Avoided Antiferromagnetic Order and Quantum Critical Point in  $\text{CeCoIn}_5$ , *Phys. Rev. Lett.* 91 (2003) 257001. doi:10.1103/PhysRevLett.91.257001.
- [45] V. A. Sidorov, M. Nicklas, P. G. Pagliuso, J. L. Sarrao, Y. Bang, A. V. Balatsky, J. D. Thompson, Superconductivity and Quantum Criticality in  $\text{CeCoIn}_5$ , *Phys. Rev. Lett.* 89 (2002) 157004. doi:10.1103/PhysRevLett.89.157004.
- [46] J. G. Analytis, H.-H. Kuo, R. D. McDonald, M. Wartenbe, P. M. C. Rourke, N. E. Hussey, I. R. Fisher, Transport near a quantum critical point in  $\text{BaFe}_2(\text{As}_{1-x}\text{P}_x)_2$ , *Nature Physics* 10 (3) (2014) 194–197. doi:10.1038/nphys2869.
- [47] V. Grinenko, K. Iida, F. Kurth, D. V. Efremov, S.-L. Drechsler, I. Cherniavskii, I. Morozov, J. Hänisch, T. Förster, C. Tarantini, J. Jaroszynski, B. Maiorov, M. Jaime, A. Yamamoto, I. Nakamura, R. Fujimoto, T. Hatano, H. Ikuta, R. Hühne, Selective mass enhancement close to the quantum critical point in  $\text{BaFe}_2(\text{As}_{1-x}\text{P}_x)_2$ , *Scientific Reports* 7 (1) (2017) 4589. doi:10.1038/s41598-017-04724-3.
- [48] Y. Nakajima, H. Shishido, H. Nakai, T. Shibauchi, K. Behnia, K. Izawa, M. Hedo, Y. Uwatoko, T. Matsumoto, R. Settai, Y. Ōnuki, H. Kontani, Y. Matsuda, Non-Fermi Liquid Behavior in the Magnetotransport of  $\text{CeMIn}_5$  (M: Co and Rh): Striking Similarity between Quasi Two-Dimensional Heavy Fermion and High-Tc Cuprates, *Journal of the Physical Society of Japan* 76 (2) (2007) 024703. doi:10.1143/JPSJ.76.024703.

- [49] T. Valla, A. V. Fedorov, P. D. Johnson, B. O. Wells, S. L. Hulbert, Q. Li, G. D. Gu, N. Koshizuka, Evidence for Quantum Critical Behavior in the Optimally Doped Cuprate  $\text{Bi}_2\text{Sr}_2\text{CaCu}_2\text{O}_{8+\delta}$ , *Science* 285 (5436) (1999) 2110–2113. doi:10.1126/science.285.5436.2110.
- [50] B. Keimer, S. A. Kivelson, M. R. Norman, S. Uchida, J. Zaanen, From quantum matter to high-temperature superconductivity in copper oxides, *Nature* 518 (7538) (2015) 179–186. doi:10.1038/nature14165.
- [51] S. Sachdev, Where is the quantum critical point in the cuprate superconductors?, *Physica Status Solidi (B)* 247 (3) (2010) 537–543. doi:10.1002/pssb.200983037.
- [52] Z. X. Zhou, S. McCall, C. S. Alexander, J. E. Crow, P. Schlottmann, A. Bianchi, C. Capan, R. Movshovich, K. H. Kim, M. Jaime, N. Harrison, M. K. Haas, R. J. Cava, G. Cao, Transport and thermodynamic properties of  $\text{Sr}_3\text{Ru}_2\text{O}_7$  near the quantum critical point, *Phys. Rev. B* 69 (2004) 140409. doi:10.1103/PhysRevB.69.140409.
- [53] S. A. Grigera, P. Gegenwart, R. A. Borzi, F. Weickert, A. J. Schofield, R. S. Perry, T. Tayama, T. Sakakibara, Y. Maeno, A. G. Green, A. P. Mackenzie, Disorder-Sensitive Phase Formation Linked to Metamagnetic Quantum Criticality, *Science* 306 (5699) (2004) 1154–1157. doi:10.1126/science.1104306.
- [54] C. Liu, V. F. C. Humbert, T. M. Bretz-Sullivan, G. Wang, D. Hong, F. Wrobel, J. Zhang, J. D. Hoffman, J. E. Pearson, J. S. Jiang, C. Chang, A. Suslov, N. Mason, M. R. Norman, A. Bhattacharya, Observation of an antiferromagnetic quantum critical point in high-purity  $\text{LaNiO}_3$ , *Nature Communications* 11 (1) (2020) 1402. doi:10.1038/s41467-020-15143-w.
- [55] D. Das, D. Gnida, P. Wiśniewski, D. Kaczorowski, Magnetic field-driven quantum criticality in antiferromagnetic  $\text{CePtIn}_4$ , *Proceedings of the National Academy of Sciences* 116 (41) (2019) 20333–20338. doi:10.1073/pnas.1910293116.
- [56] S. Sachdev, *Quantum Phase Transitions*, 2nd Edition, Cambridge University Press, 2011. doi:10.1017/CB09780511973765.

- [57] A. A. Kordyuk, Pseudogap from ARPES experiment: Three gaps in cuprates and topological superconductivity (Review Article), *Low Temperature Physics* 41 (5) (2015) 319–341. doi:10.1063/1.4919371.
- [58] O. Cyr-Choinière, R. Daou, F. Laliberté, C. Collignon, S. Badoux, D. LeBoeuf, J. Chang, B. J. Ramshaw, D. A. Bonn, W. N. Hardy, R. Liang, J.-Q. Yan, J.-G. Cheng, J.-S. Zhou, J. B. Goodenough, S. Pyon, T. Takayama, H. Takagi, N. Doiron-Leyraud, L. Taillefer, Pseudogap temperature  $T^*$  of cuprate superconductors from the Nernst effect, *Phys. Rev. B* 97 (2018) 064502. doi:10.1103/PhysRevB.97.064502.
- [59] E. J. Calegari, A. C. Lausmann, S. G. Magalhaes, C. M. Chaves, A. Troper, Pseudogap and the specific heat of high  $T_c$  superconductors: a Hubbard model in a  $n$ -pole approximation, *Journal of Physics: Conference Series* 592 (2015) 012075. doi:10.1088/1742-6596/592/1/012075.
- [60] D. F. Agterberg, J. S. Davis, S. D. Edkins, E. Fradkin, D. J. Van Harlingen, S. A. Kivelson, P. A. Lee, L. Radzihovsky, J. M. Tranquada, Y. Wang, *The Physics of Pair-Density Waves: Cuprate Superconductors and Beyond*, *Annual Review of Condensed Matter Physics* 11 (1) (2020) 231–270. doi:10.1146/annurev-conmatphys-031119-050711.
- [61] P. Choubey, S. H. Joo, K. Fujita, Z. Du, S. D. Edkins, M. H. Hamidian, H. Eisaki, S. Uchida, A. P. Mackenzie, J. Lee, J. C. S. Davis, P. J. Hirschfeld, Atomic-scale electronic structure of the cuprate pair density wave state coexisting with superconductivity, *Proceedings of the National Academy of Sciences* (2020). doi:10.1073/pnas.2002429117.
- [62] S. Badoux, W. Tabis, F. Laliberté, G. Grissonnanche, B. Vignolle, D. Vignolles, J. Béard, D. A. Bonn, W. N. Hardy, R. Liang, N. Doiron-Leyraud, L. Taillefer, C. Proust, Change of carrier density at the pseudogap critical point of a cuprate superconductor, *Nature* 531 (7593) (2016) 210–214. doi:10.1038/nature16983.
- [63] D. LeBoeuf, N. Doiron-Leyraud, B. Vignolle, M. Sutherland, B. J. Ramshaw, J. Levallois, R. Daou, F. Laliberté, O. Cyr-Choinière, J. Chang, Y. J. Jo, L. Balicas, R. Liang, D. A. Bonn, W. N. Hardy,

- C. Proust, L. Taillefer, Lifshitz critical point in the cuprate superconductor  $\text{YBa}_2\text{Cu}_3\text{O}_y$  from high-field Hall effect measurements, *Phys. Rev. B* 83 (2011) 054506. doi:10.1103/PhysRevB.83.054506.
- [64] N. Doiron-Leyraud, S. Badoux, S. René de Cotret, S. Lepault, D. LeBoeuf, F. Laliberté, E. Hassinger, B. J. Ramshaw, D. A. Bonn, W. N. Hardy, R. Liang, J.-H. Park, D. Vignolles, B. Vignolle, L. Taillefer, C. Proust, Evidence for a small hole pocket in the Fermi surface of underdoped  $\text{YBa}_2\text{Cu}_3\text{O}_y$ , *Nature Communications* 6 (1) (2015) 6034. doi:10.1038/ncomms7034.
- [65] F. Laliberté, J. Chang, N. Doiron-Leyraud, E. Hassinger, R. Daou, M. Rondeau, B. J. Ramshaw, R. Liang, D. A. Bonn, W. N. Hardy, S. Pyon, T. Takayama, H. Takagi, I. Sheikin, L. Malone, C. Proust, K. Behnia, L. Taillefer, Fermi-surface reconstruction by stripe order in cuprate superconductors, *Nature Communications* 2 (1) (2011) 432. doi:10.1038/ncomms1440.
- [66] D. Haug, V. Hinkov, Y. Sidis, P. Bourges, N. B. Christensen, A. Ivanov, T. Keller, C. T. Lin, B. Keimer, Neutron scattering study of the magnetic phase diagram of underdoped  $\text{YBa}_2\text{Cu}_3\text{O}_{6+x}$ , *New Journal of Physics* 12 (10) (2010) 105006. doi:10.1088/1367-2630/12/10/105006.
- [67] M. Presland, J. Tallon, R. Buckley, R. Liu, N. Flower, General trends in oxygen stoichiometry effects on  $T_c$  in Bi and Tl superconductors, *Physica C: Superconductivity* 176 (1) (1991) 95 – 105.
- [68] M. Hücker, N. B. Christensen, A. T. Holmes, E. Blackburn, E. M. Forgan, R. Liang, D. A. Bonn, W. N. Hardy, O. Gutowski, M. v. Zimmermann, S. M. Hayden, J. Chang, Competing charge, spin, and superconducting orders in underdoped  $\text{YBa}_2\text{Cu}_3\text{O}_y$ , *Phys. Rev. B* 90 (2014) 054514. doi:10.1103/PhysRevB.90.054514.
- [69] S. Blanco-Canosa, A. Frano, E. Schierle, J. Porras, T. Loew, M. Minola, M. Bluschke, E. Weschke, B. Keimer, M. Le Tacon, Resonant x-ray scattering study of charge-density wave correlations in  $\text{YBa}_2\text{Cu}_3\text{O}_{6+x}$ , *Phys. Rev. B* 90 (2014) 054513. doi:10.1103/PhysRevB.90.054513.
- [70] P. Coleman, A. J. Schofield, Quantum criticality, *Nature* 433 (7023) (2005) 226–229. doi:10.1038/nature03279.

- [71] T. Degen, M. Sadki, E. Bron, U. König, G. Nénert, The HighScore suite, Powder Diffraction 29 (S2) (2014) S13 – S18. doi:10.1017/S0885715614000840.
- [72] V. Petříček, M. Dušek, L. Palatinus, Crystallographic Computing System JANA2006: General features, Zeitschrift für Kristallographie - Crystalline Materials 229 (5) (2014) 345–352. doi:doi:10.1515/zkri-2014-1737.
- [73] H. M. Rietveld, Line profiles of neutron powder-diffraction peaks for structure refinement, Acta Crystallographica 22 (1) (1967) 151–152. doi:10.1107/S0365110X67000234.
- [74] H. M. Rietveld, A profile refinement method for nuclear and magnetic structures, Journal of Applied Crystallography 2 (2) (1969) 65–71. doi:10.1107/S0021889869006558.
- [75] A. Le Bail, H. Duroy, J. Fourquet, Ab-initio structure determination of  $\text{LiSbWO}_6$  by X-ray powder diffraction, Materials Research Bulletin 23 (3) (1988) 447–452. doi:https://doi.org/10.1016/0025-5408(88)90019-0.
- [76] L. Xie, T. Su, X. Li, Magnetic field dependence of Schottky anomaly in the specific heats of stripe-ordered superconductors  $\text{La}_{1.6-x}\text{Nd}_{0.4}\text{Sr}_x\text{CuO}_4$ , Physica C: Superconductivity 480 (2012) 14 – 18.
- [77] We have estimated the  $C/T$  of this material using temperature dependence of  $\text{BaSO}_4$  and the fact that at room temperature the standard molar entropy 132.2 J/(mol K) of it corresponds to  $C_{\text{BaSO}_4} = 101.8$  J/(mol K) (CRC Handbook of Chemistry and Physics, 95 edition, CRC 2014, pp.4-50). At the same temperature, the standard molar entropy of  $\text{BaSeO}_4$  is 134 J/(mol K) (<http://chemister.ru/Database/properties-en.php?dbid=1&id=7158>), so that its heat capacity should not be much different from  $\text{BaSO}_4$ .
- [78] N. I. Matskevich, Y. F. Minenkov, G. A. Berezovskii, Thermodynamic properties of yttrium cuprate, arXiv.1401.7422 (2014). URL <https://arxiv.org/abs/1401.7422>

- [79] D. Eckert, A. Junod, T. Graf, J. Muller, Low Temperature specific heat of  $\text{YBa}_3\text{Cu}_2\text{O}_7$ ,  $\text{Y}_2\text{BaCuO}_5$ ,  $\text{CuO}$  and  $\text{BaCuO}_{2+x}$ , *Physica C: Superconductivity* 153-155 (1988) 1038 – 1039.
- [80] J.-Y. Lin, Y. S. Hsieh, D. A. Chareev, A. N. Vasiliev, Y. Parsons, H. D. Yang, Coexistence of isotropic and extended  $s$ -wave order parameters in  $\text{FeSe}$  as revealed by low-temperature specific heat, *Phys. Rev. B* 84 (2011) 220507. doi:10.1103/PhysRevB.84.220507.
- [81] D. C. Carless, H. E. Hall, J. R. Hook, Vibrating wire measurements in liquid  $^3\text{He}$  II. The superfluid B phase, *Journal of Low Temperature Physics* 50 (5) (1983) 605–633. doi:10.1007/BF00683498.
- [82] S. J. Collocott, R. Driver, L. Dale, S. X. Dou, Schottky anomaly in the heat capacity of the high- $T_c$  superconductor  $\text{YBa}_2\text{Cu}_3\text{O}_7$ , *Phys. Rev. B* 37 (1988) 7917–7919. doi:10.1103/PhysRevB.37.7917.
- [83] G. Mu, Y. Wang, L. Shan, H.-H. Wen, Possible nodeless superconductivity in the noncentrosymmetric superconductor  $\text{Mg}_{12-\delta}\text{Ir}_{19}\text{B}_{16}$ , *Phys. Rev. B* 76 (2007) 064527. doi:10.1103/PhysRevB.76.064527.